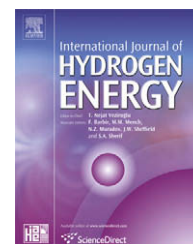


Available at www.sciencedirect.comjournal homepage: www.elsevier.com/locate/he

Radiation characteristics of *Chlamydomonas reinhardtii* CC125 and its truncated chlorophyll antenna transformants *tla1*, *tlaX* and *tla1-CW*⁺

Halil Berberoglu^a, Laurent Pilon^{a,*}, Anastasios Melis^b

^aMechanical and Aerospace Engineering Department, Henry Samueli School of Engineering and Applied Science, University of California, Los Angeles, CA 90095, USA

^bDepartment of Plant and Microbial Biology, University of California, Berkeley, CA 94720, USA

ARTICLE INFO

Article history:

Received 31 August 2007

Received in revised form

17 July 2008

Accepted 19 July 2008

Available online 16 October 2008

Keywords:

photobiological hydrogen

chlorophyll antenna

genetic engineering

absorption

scattering

chlamydomonas reinhardtii

ABSTRACT

This experimental study reports, for the first time, the radiation characteristics of the unicellular green algae *Chlamydomonas reinhardtii* strain CC125 and its truncated chlorophyll antenna transformants *tla1*, *tlaX* and *tla1-CW*⁺. Photobiological hydrogen production is a sustainable alternative to thermo-chemical and electrolytic technologies with the possible advantage of carbon dioxide mitigation. However, scale-up of photobioreactors from bench top to industrial scale is made difficult by excessive absorption and waste of light energy as heat and fluorescence. This results in limited light penetration into the photobioreactor and low solar to hydrogen energy conversion efficiency. To overcome these challenges, the algae *C. reinhardtii* have been genetically engineered with reduced pigment concentrations in their photosystems. This can improve the performance of photobioreactors by increasing the saturation irradiance of algae and quantum efficiency of photobiological hydrogen production.

The extinction and absorption coefficients of all strains studied are obtained from normal-normal and normal-hemispherical transmittance measurements over the spectral range from 300 to 1300 nm. Moreover, a polar nephelometer is used to measure the scattering phase function of the microorganisms at 632.8 nm. It is established that the wild strain *C. reinhardtii* CC125 has major absorption peaks at 435 and 676 nm, corresponding to the in vivo absorption peaks of chlorophyll *a*, and at 475 and 650 nm corresponding to those of chlorophyll *b*. The genetically engineered strains have less chlorophyll pigments than the wild strain and thus have smaller absorption cross-sections. In particular, the mutant *tlaX* features a significant reduction in chlorophyll *b* concentration. For all mutants, however, the reduction in the absorption cross-section is accompanied by an increase in scattering cross-section. Although scattering becomes the dominant phenomenon contributing to the overall extinction of light, it is mainly in the forward direction. Thus, to fully assess the effect of genetic engineering on light transport in the photobioreactor requires careful radiation transfer analysis using the radiation characteristics reported in this study.

© 2008 International Association for Hydrogen Energy. Published by Elsevier Ltd. All rights reserved.

* Corresponding author. Tel.: +1 (310) 206 5598; fax: +1 (310) 206 4830.

E-mail address: pilon@seas.ucla.edu (L. Pilon).

0360-3199/\$ – see front matter © 2008 International Association for Hydrogen Energy. Published by Elsevier Ltd. All rights reserved.
doi:10.1016/j.ijhydene.2008.07.071

Nomenclature			
a	scattering particle diameter (m)	z	distance between the detector and the virtual image of the last lens (m)
$A_{\text{abs},\lambda}$	spectral mass absorption cross-section ($\text{m}^2 \text{kg}^{-1}$)	<i>Greek symbols</i>	
$E_{\text{ext},\lambda}$	spectral mass extinction cross-section ($\text{m}^2 \text{kg}^{-1}$)	β	extinction coefficient (m^{-1})
f_1	weighing factor in TPF	ϵ_{h}	contribution of the forward scattered light to $T_{\text{h},\lambda,x}$
g	Henyey–Greenstein asymmetry factor	ϵ_{n}	contribution of the forward scattered light to $T_{\lambda,x}$
h_1	weighing factor in TPF	Θ	scattering angle (rad)
I	radiance (intensity) ($\text{W m}^{-2} \text{sr}^{-1}$)	Θ_{a}	half acceptance angle of the detector (rad)
L	coordinate direction, Fig. 4b	κ	absorption coefficient (m^{-1})
l_{p}	photon path length (m)	λ	wavelength (nm)
n	refractive index	Ω	solid angle (sr)
OD	optical density	σ	scattering coefficient (m^{-1})
P	pathlength, $P = w/2 \sin \Theta + r$	τ	optical thickness
r	the radius of rotation of the fiber-optic probe (m)	Φ	scattering phase function
\hat{s}	local spatial coordinate unit vector	χ	apparent(uncorrected) extinction coefficient (m^{-1})
$S_{\text{sca},\lambda}$	spectral mass scattering cross-section of microorganisms ($\text{m}^2 \text{kg}^{-1}$)	χ_{h}	apparent(uncorrected) absorption coefficient (m^{-1})
t	sample thickness (m)	<i>Subscripts</i>	
T	transmittance (%)	λ	refers to wavelength
U	correction term in recovering the phase function, Eq. (12)	h	refers to normal-hemispherical measurements
w	incident beam diameter (m)	HG	refers to Henyey–Greenstein phase function
X	microorganism concentration (kg m^{-3})	PBS	refers to phosphate buffer saline solution
x	size parameter	TPF	refers to truncated phase function

1. Introduction

Photobioreactors are enclosures used for cultivating microorganisms that utilize sunlight as their energy source for their growth and subsequent product formation [1]. They have been used in environmental engineering such as wastewater treatment, heavy metal removal and CO₂ mitigation [2]. More recently, they have also been considered for hydrogen production [3–7]. In photobiological hydrogen production, the presence of dissolved O₂ in the liquid medium and limited sunlight penetration through a high-density culture are the major issues limiting the solar energy conversion efficiency [8–12]. The former has been alleviated by reversibly shutting down the O₂ production metabolism of the unicellular green algae *Chlamydomonas reinhardtii* by sulphur deprivation [13]. This establishes *C. reinhardtii* as one of the best candidates for photobiological hydrogen production [8,9,13]. However, limited solar radiation penetration remains a challenge that affects the H₂ production rate and the solar to H₂ energy conversion efficiency of large cell density mass cultures.

Solar radiation transfer within absorbing, scattering and non-emitting media, such as microorganism suspensions in photobioreactors, is governed by the radiative transport equation (RTE) [14]. The RTE is a semi-empirical integro-differential equation derived from energy conservation considerations. For a given wavelength λ , it is expressed in terms of dimensionless optical coordinates as [15]

$$\frac{dI_{\lambda}}{d\tau_{\lambda}} = -I_{\lambda}(\tau_{\lambda}, \hat{s}) + \frac{\omega_{\lambda}}{4\pi} \int_{4\pi} I_{\lambda}(\tau_{\lambda}, \hat{s}_i) \Phi_{\lambda}(\hat{s}_i, \hat{s}) d\Omega_i \quad (1)$$

where I_{λ} is the spectral radiance (sometimes known as spectral intensity [15]) expressed in $\text{W m}^{-2} \text{sr}^{-1}$. Here, \hat{s} is the unit vector in the line-of-sight direction and $d\Omega_i$ is the solid angle around \hat{s}_i . The dimensionless optical thickness τ_{λ} and the single scattering albedo ω_{λ} are defined, respectively, as

$$\tau_{\lambda} = \int_0^s (\kappa_{\lambda} + \sigma_{\lambda}) ds = \int_0^s \beta_{\lambda} ds \quad (2)$$

and

$$\omega_{\lambda} = \frac{\sigma_{\lambda}}{\kappa_{\lambda} + \sigma_{\lambda}} = \frac{\sigma_{\lambda}}{\beta_{\lambda}} \quad (3)$$

where κ_{λ} , σ_{λ} and β_{λ} ($=\kappa_{\lambda} + \sigma_{\lambda}$) are the absorption, scattering and extinction coefficients, respectively and expressed in m^{-1} . The scattering phase function $\Phi_{\lambda}(\hat{s}_i, \hat{s})$ represents the probability that the radiation propagating in direction \hat{s}_i be scattered in direction \hat{s} and is normalized such that

$$\frac{1}{4\pi} \int_{4\pi} \Phi_{\lambda}(\hat{s}_i, \hat{s}) d\Omega_i = 1 \quad (4)$$

Note that the variables κ_{λ} , σ_{λ} , β_{λ} and Φ_{λ} are often denoted by a_{λ} , b_{λ} , c_{λ} and β_{λ} , respectively, in the ocean optics literature [16–18]. In the present study, the nomenclature commonly used in the radiative heat transfer community is employed [15].

Eq. (1) indicates that the absorption and scattering coefficients, or the extinction coefficient and the single scattering albedo, together with the scattering phase function are major parameters needed to solve the radiation transfer equation and predict light transfer in photobioreactors for simulation, design and optimization purposes. However, these characteristics are

strongly dependent on wavelength and difficult to predict from electromagnetic wave theory given the complex morphology of the microorganisms and their various chromophores.

Moreover, wild-type strains of algae found in nature contain more light harvesting pigments than necessary for the saturation of photosynthesis under bright sunlight, which is a survival strategy due to limited light in their natural habitats [19]. However, this is disadvantageous in scaled-up photobioreactors because (i) the algae close to the light source will absorb more light than they can utilize and waste it and (ii) light will not penetrate deep into the photobioreactor resulting in a reduction of the system efficiency. In order to overcome these challenges, Polle et al. [19] genetically engineered the green algae *C. reinhardtii* to have less pigments by truncating their chlorophyll antenna. The authors demonstrated that the saturation irradiance of photosynthesis was increased by approximately a factor 2 from about 1500 to 3000 $\mu\text{mol m}^{-2} \text{s}^{-1}$.

Qualitatively, the genetic transformation is apparent to the unaided eye as the genetically engineered strains appear light green while the wild strain appears dark green. This study aims at quantitatively assessing the effect of genetic engineering on the radiation characteristics of *C. reinhardtii* CC125 and its truncated chlorophyll antenna transformants *tla1*, *tlaX* and *tla1-CW*⁺.

2. Current state of knowledge

2.1. Truncated chlorophyll antenna transformants

Photochemical reactions conducted by algae start with the absorption of solar light by the pigments in the light harvesting chlorophyll antenna complexes [20]. Besides having a chlorophyll *a* containing core antenna complex, *C. reinhardtii* also has a chlorophyll *b* containing auxiliary light-harvesting antenna [20]. These complexes channel the solar energy to two distinct photosystems, namely photosystems I and II (PSI and PSII), where electrons necessary for driving various chemical reactions are generated from oxidation of water [21]. In *C. reinhardtii* wild strain, PSI and PSII are reported to contain 240 and 230 chlorophyll molecules, respectively [8]. However, for proper functioning of these complexes under bright sunlight, the algae need only 95 and 37 chlorophyll molecules in the core complexes of PSI and PSII, respectively [13]. Polle et al. [20] genetically engineered *C. reinhardtii* via DNA insertional mutagenesis to obtain the mutant strain *tla1* having permanently reduced number of chlorophyll molecules per photosystem. This strain was derived from a cell wall-less strain CC425-CW⁻ and did not contain cell wall [20]. For use in photobioreactors, it is necessary that cells have walls so that they do not break on mechanical stirring [20]. Thus, Polle et al. [20] crossed *tla1* with a cell wall containing strain CC1068 and isolated the strain *tla1-CW*⁺ showing observable characteristics (phenotype) of *tla1* and having a cell wall. The strain CC125 is the wild-type *C. reinhardtii* and is used as a reference to compare the radiation characteristics of the genetically engineered strains. Finally, the strain *tlaX* has even a smaller chlorophyll antenna than *tla1*. At the time of preparation of the manuscript no publications were available on the mutant *tlaX*. The reduction in pigment concentration compared with *tla1* is evident to the naked eye.

2.2. Measurement of the radiation characteristics

The radiation characteristics of microorganisms are measured under the single scattering regime [22]. This means that the scattered light undergoes only one scattering event in the sampling volume. This condition is satisfied if the sample thickness *t* is much smaller than the photon mean free path *l_p*, such that [23,24],

$$t(1 - g_\lambda) \ll l_{p,\lambda} \quad (5)$$

where $l_{p,\lambda} = 1/\beta_\lambda$ and g_λ is the mean cosine of the scattering angle. The latter is also known as the Henyey–Greenstein asymmetry factor and is defined as [15],

$$g_\lambda = \frac{1}{4\pi} \int_{4\pi} \Phi_\lambda(\theta) \cos\theta \, d\Omega \quad (6)$$

Under single scattering regime, the radiation characteristics of microorganisms are linearly dependent on concentration [14]. Thus, it is more convenient to introduce the mass extinction and absorption cross-sections, denoted by $E_{\text{ext},\lambda}$ and $A_{\text{abs},\lambda}$, respectively, and expressed in meter square per kilogram. They are defined as [14],

$$E_{\text{ext},\lambda} = \frac{\beta_\lambda}{X} \quad \text{and} \quad A_{\text{abs},\lambda} = \frac{\kappa_\lambda}{X} \quad (7)$$

where *X* is the concentration of the microorganisms, expressed in kilogram dry cell weight per cubic meter of liquid medium. Similarly, the scattering coefficient σ_λ and the mass scattering cross-section $S_{\text{sca},\lambda}$ expressed in meter square per kilogram are defined as,

$$\sigma_\lambda = \beta_\lambda - \kappa_\lambda \quad \text{and} \quad S_{\text{sca},\lambda} = \frac{\sigma_\lambda}{X} \quad (8)$$

The extinction coefficient β_λ is obtained from normal–normal transmittance measurements of dilute suspensions [15]. The most common technique uses a spectrophotometer where a collimated monochromatic beam is incident on a cuvette containing the algal suspension [15]. The transmitted light is focused onto a pinhole in front of the detector to eliminate the light scattered in directions other than the normal direction [25]. Bohren and Huffman [25] indicated that for reliable measurement of the extinction coefficient of highly forward scattering samples, the half acceptance angle of the detector θ_a has to satisfy

$$\theta_a < \frac{1}{2x_\lambda} \quad (9)$$

where x_λ is the size parameter defined as [15],

$$x_\lambda = \frac{2\pi a n_\lambda}{\lambda} \quad (10)$$

Here, *a* is the scattering particle radius, n_λ is the refractive index of the non-absorbing and non-scattering medium in which the scatterers are submerged. Furthermore, to eliminate the effects of diffraction and multiple reflections from the container walls, the measurements are taken with respect to a cuvette containing the above-mentioned medium alone. In a different technique, Daniel and Incropera [26] measured the extinction coefficient of unicellular green algae *Chlorella pyrenoidosa* using a fiber-optic probe submerged in the microorganism suspension; thus, eliminating possible reflection and refraction by the container walls. The probe had

a half angle of view of 1.28° (in water) and the sample was illuminated by a collimated beam of diameter 71 mm (Xenon Arc Lamp).

Moreover, a large body of literature exists on measuring the absorption coefficient κ_λ both in the field (in situ) and in the laboratory. In situ measurements usually deal with extremely small concentration of microorganisms and are designed to overcome this difficulty by increasing the path length of the sample. Some of these methods include:

- *Reflecting tube absorption meter.* This technique uses a tube with reflective walls as the sample holder [27,28]. The tube is illuminated with collimated monochromatic light at one end. As the light propagates through the sample it gets absorbed and scattered. The scattered light is reflected from walls and detected at the other end together with the transmitted light. The optical pathlength of the detected scattered light is larger than that of the transmitted light resulting in over estimation of the absorption coefficient.
- *Isotropic point source techniques.* This technique relies on the principle that irradiance from an isotropic point source decays proportional to $\exp(-\kappa R)/R^2$, where R is the radial distance from the source [29]. Thus, the absorption coefficient can be obtained by measuring the irradiance at different radial distances from the source. This method is valid under single scattering regime and enables the measurement of small absorption coefficients of natural waters.

Furthermore, some of the laboratory techniques for measuring the absorption coefficient include the following:

- *Integrating cavity absorption meter.* This technique uses a special sample holder known as the integrating cavity made of two concentric cavities separated by a diffuse translucent wall [30]. The sample is contained in the innermost cavity and is illuminated homogeneously from all directions with monochromatic light delivered by a set of fiber-optics. The attenuated light is detected by two sets of fiber-optics at two different radial locations with respect to the sample. The device is calibrated with Irgalan Black and Alcian Blue solutions of known absorption characteristics taking into account the geometry of the device. This device is regarded as one of the most accurate methods for measuring the absorption coefficient [24].
- *Photoacoustic technique.* In this technique, the sample is irradiated with a beam of light chopped at some arbitrary frequency [15]. The absorbed light is dissipated as heat causing periodic changes in sample temperature. These temperature changes give rise to pressure oscillations that can be detected by a microphone and correlated to the absorption coefficient of the particles [31].
- *Integrating sphere technique.* This method relies on the fact that microorganism suspensions scatter light strongly in the forward direction [14,22,26]. Thus, a significant portion of the forward scattered radiation is collected by the integrating sphere that has a large acceptance angle. Thus, the attenuation in the transmitted radiation is attributed solely to the effect of absorption. However, absorption coefficient obtained with this method suffers from scattering error [17,32,33]. Several correction methods have been suggested by

Davies-Colley et al. [17], Merzlyak and Naqvi [34], and Stramski and Piskozub [33]. The method reported by Davies-Colley et al. [17] will be explained in detail in the next section.

Finally, the scattering phase function ϕ_λ is measured using a nephelometer [25]. A typical nephelometer is comprised of a detector with a small acceptance angle that can measure the scattered radiation as a function of the polar and the azimuthal angles. A recent review of different nephelometer designs was given by Jonasz and Fournier [24]. For spherical or randomly oriented particles, as in the case of well-mixed microorganism suspensions, the phase function does not change as a function of the azimuthal angle [15]. Thus, most nephelometers measure ϕ_λ as a function of the polar angle θ only. Moreover, the scattering phase function for large particles does not vary significantly with wavelength at scattering angles less than 15° [16]. Since most of the scattered light is in the forward direction, phase function measurements taken at 632.8 nm can be used as a first approximation for modeling light transfer in photobioreactors over the photosynthetically active region (PAR) ranging from 400 to 700 nm.

To the best of our knowledge, this work presents, for the first time, experimental measurements of the radiation characteristics of the hydrogen producing green algae *C. reinhardtii* CC125 and its truncated chlorophyll antenna transformants *tla1*, *tlaX* and *tla1-CW⁺* over the spectral range from 300 to 1300 nm as well as their scattering phase function at 632.8 nm.

3. Materials and methods

3.1. Microorganism cultivation and sample preparation

C. reinhardtii is a unicellular green algae in the shape of a spheroid measuring about 10 μm in diameter. All strains were cultivated heterotrophically under aerobic conditions in TAP medium [36] with irradiance of 2000–3000 lx provided by fluorescent light bulbs (Ecologic by Sylvania, USA). The pH of the medium was 7.3. Samples were taken from actively growing cultures of each strain during their exponential growth phase. In order to eliminate absorption and scattering due to the nutrient media, the microorganisms were centrifuged at 2000 rpm for 5 min (Super T21 by Sorvall, USA), washed and suspended in phosphate buffer saline (PBS) solution. While measuring their radiation characteristics, the microorganisms should not be suspended in distilled water [37]. Indeed, due to the large osmotic gradient between the inside of the cells and pure water, the cells will absorb water and stretch, with a concomitant change in their radiation characteristics. However, PBS solution overcomes this problem and provides a non-scattering medium, suitable for optical measurements [37]. One liter of PBS solution contained 8 g NaCl, 0.2 g KCl, 1.15 g $\text{Na}_2\text{HPO}_4 \cdot 7\text{H}_2\text{O}$ and 0.2 g KH_2PO_4 . The refractive index of the PBS solution was measured with an abbe refractometer (Leica USA, Model Mark II Plus) and found to be 1.3341 at 21°C .

Fig. 1 shows the in vivo differential interference contrast (DIC) and chlorophyll fluorescence micrographs of all strains. The images were obtained using Zeiss 510 confocal scanning laser microscope in the transmission and epi-fluorescence

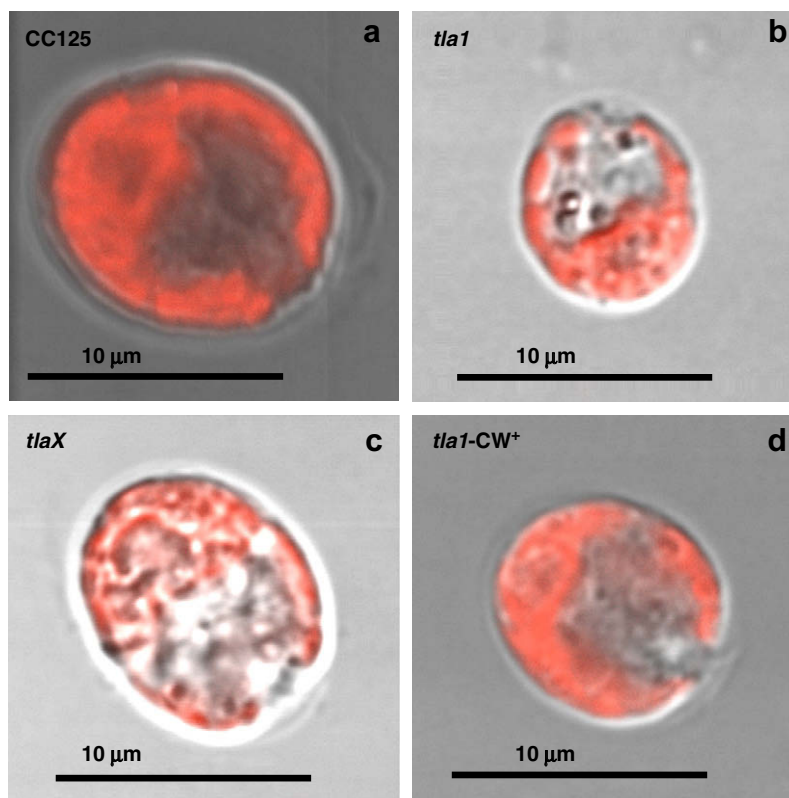


Fig. 1 – Differential interference contrast and fluorescence micrographs of (a) CC125, (b) *tla1*, (c) *tlaX* and *tla1-CW*⁺. The scale bars correspond to 10 μm . Chlorophyll pigments fluoresce in red.

mode simultaneously as reported by Chen and Melis [38]. The excitation was provided by a Helium Neon laser at 543 nm while the chlorophyll fluorescence emission was detected in the red region with a long pass filter with a cut-off wavelength of 560 nm placed in front of the detector. It illustrates the size and shape of each strain as well as the location of the chlorophyll pigments that fluoresce in red [36]. The strong red fluorescence observed in the wild strain CC125 qualitatively shows that it has the largest concentration of chlorophyll while *tlaX* has the least. In addition, the cell size distribution has been quantified for each strain using a 100 μm deep hemacytometer (Hausser Scientific, USA, Model 1490) and the image processing and analysis software ImageJ [39]. The software approximates the cells as ellipses and reports the primary and secondary axes as major and minor diameters. For each strain, over 400 cells were counted. Fig. 2 shows the number frequency of the major and minor diameters of the cells for all strains with bins of width 0.1 μm . It indicates that *tla1* has the smallest mean major and minor diameters of 8.4 and 7.4 μm , respectively, whereas those of *tla1-CW*⁺ were largest and equal to 10.3 and 8.9 μm . Moreover, *tlaX* had the largest standard deviation of 2.4 and 2.6 μm for the major and minor diameters, respectively. The mean major and minor diameters along with their standard deviations have been summarized in Table 1. In addition, Table 1 reports (i) the circularity defined as $4\pi(\text{area of the cell}/\text{perimeter of the cell})^2$ [39], and (ii) the Ferret diameters defined as the longest distance between two points along the perimeter of a particle [39], for all strains. Note that observations under the optical

microscope establish that the size and the shape of all strains investigated remain the same in PBS as in the nutrient media.

Three dilutions of each strain were prepared. Microorganism concentration of each dilution was determined using calibration curves that relate the optical density (OD) at 750 nm of a microorganism suspension to both the dry cell weight and the number of cells per unit volume of liquid [36]. The optical density is defined as $\text{OD} = -\log_{10}(T_{750}/T_{750,\text{PBS}})$, where T_{750} and $T_{750,\text{PBS}}$ are the transmittance at 750 nm of the microorganism suspension in PBS and of PBS alone, respectively. The calibration curves were created by measuring the dry cell weight and the number of cells per unit volume at a given OD. First, the OD of the microorganisms was measured in disposable polystyrene cuvettes with light path of 10 mm at 750 nm [40] using a UV-VIS spectrophotometer (Cary-3E by Varian, USA). Then, the cells were counted using the hemacytometer and ImageJ software. Finally, the microorganism suspensions were filtered through mixed cellulose filter membranes with 0.45 μm pore size (HAWP-04700 by Millipore, USA) and dried at 85 $^{\circ}\text{C}$ over night. The dried filters were weighed immediately after being taken out of the oven on a precision balance (model AT261 by Delta Range Factory, USA) with a precision of 0.01 mg. Fig. 3(a) and (b) show the dry cell weight in kilogram dry cell per cubic meter and the number density in number of cells per cubic meter, respectively, versus OD at 750 nm calibration curves for all strains using a 1 cm pathlength cuvette. It indicates that for all strains, 1 unit of OD at 750 nm corresponds to a microorganism concentration of 0.367 kg dry cell m^{-3} and 2.79×10^6 cells m^{-3} .

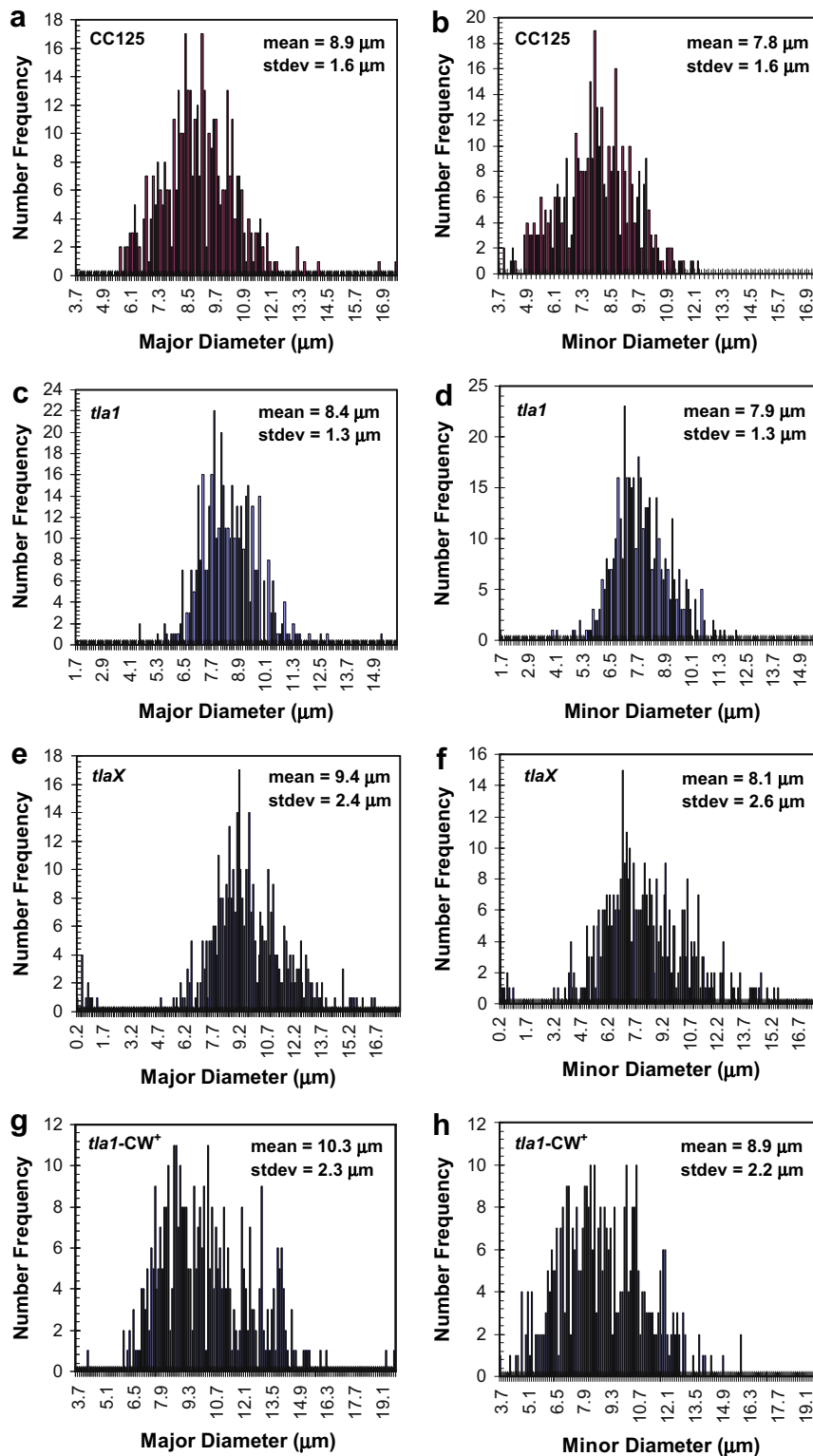


Fig. 2 – Number frequency of the major and minor cell diameters of (a,b) CC125, (c,d) *tla1*, (e,f) *tlaX*, and (g,h) *tla1-CW⁺*.

Finally, the chlorophyll *a* and chlorophyll *b* concentrations were determined for each strain using the ethanol extraction method developed by Wintermans and De Mots [35]. Table 2 summarizes the chlorophyll *a*, chlorophyll *b*, and total chlorophyll concentrations for all strains in gram of chlorophyll per kilogram dry cell of microorganism. It indicates that all

genetically engineered strains indeed contain both less chlorophyll *a* and *b* than the wild strain. Moreover, CC125, *tla1*, and *tla1-CW⁺* had half as much chlorophyll *b* than chlorophyll *a* whereas strain *tlaX* had about hundred times less chlorophyll *b* than chlorophyll *a*. Note that *tla1-CW⁺* has more chlorophyll *a* and *b* than *tla1*. This is most likely due to the fact

Table 1 – Mean diameters, their standard deviations, circularity, and Ferret diameters of all strains

	CC125	tla1	tlaX	tla1-CW ⁺
Average major diameter (μm)	8.9	8.4	9.4	10.3
Standard deviation of major diameter (μm)	1.6	1.3	2.4	2.3
Average minor diameter (μm)	7.8	7.9	8.1	8.9
Standard deviation of minor diameter (μm)	1.6	1.3	2.6	2.2
Circularity	0.86	0.9	0.8	0.8
Feret diameter (μm)	9.2	8.8	9.8	10.6

that tla1-CW⁺ was an offspring of tla1 and the wild strain CC1068 [19]. Overall, these results corroborate with qualitative observations made in Fig. 1.

3.2. Experimental procedure and analysis

In measuring the radiation characteristics, the following assumptions are made: (1) the microorganisms are well mixed

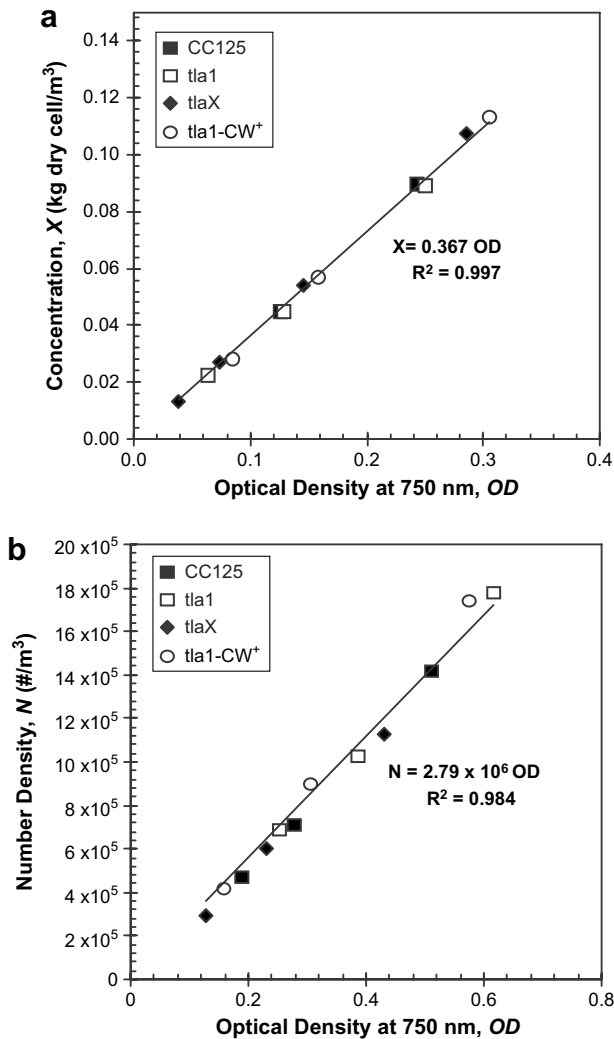


Fig. 3 – Calibration curves of (a) dry cell weight and (b) number density versus optical density (OD) at 750 nm for all strains.

Table 2 – Chlorophyll (Chl) concentrations of all *C. reinhardtii* strains determined by ethanol extraction [36]

Strain	Chl a (g kg ⁻¹ dry cell)	Chl b (g kg ⁻¹ dry cell)	Total Chl (g kg ⁻¹ dry cell)
CC125	29.80 ± 2.03	14.53 ± 1.11	44.33 ± 3.14
tla1	18.98 ± 1.36	8.67 ± 0.66	27.65 ± 2.02
tlaX	16.82 ± 0.24	0.16 ± 0.07	16.98 ± 0.31
37RP-tla1	22.24 ± 2.17	10.34 ± 0.98	32.57 ± 3.15

and randomly oriented, (2) for all measurements, the path-length and the concentration of the samples is such that single scattering prevails, i.e., photons undergo one scattering event at most as they travel through the suspension, (3) the scattering phase function has azimuthal symmetry and is only a function of the polar angle, and (4) the scattering phase function is independent of wavelength in the spectral range of interest from 300 to 1300 nm.

First, a polar nephelometer has been constructed to experimentally measure the scattering phase function of microorganisms at 632.8 nm. The details of the experimental set-up and its validation have been reported elsewhere [41] and need not be repeated. The nephelometer featured a fiber optic probe with a miniature Gershun tube that limits the half acceptance angle of the detector to 0.7° in water. The nephelometer measured the scattered intensity I_λ in $W m^{-2} sr^{-1}$ as a function of the polar angle θ . The scattering phase function was recovered using the analysis suggested by Privoznik et al. [22],

$$\Phi_\lambda(\theta) = \frac{2I_\lambda(\theta)[U_\lambda(\theta)]^{-1}}{\int_0^\pi I_\lambda(\theta)[U_\lambda(\theta)]^{-1} \sin \theta d\theta} \quad (11)$$

The geometrical correction term $U_\lambda(\theta)$ accounts for the variation of the scattering volume and the pathlength between the scattering volume center and the detector with detection angle and is given by [22],

$$U_\lambda(\theta) = \int_0^{w/\sin \theta} \left[1 + \beta_\lambda \frac{w}{2} c \tan \theta - \beta_\lambda L \cos \theta \right] \times \left[1 - \beta_\lambda \left(r - \frac{w}{2 \sin \theta} \right) \right] \left[1 - \beta_\lambda \left(\frac{w}{\sin \theta} - L \right) \right] dL \quad (12)$$

where w is the beam diameter equal to 1.7×10^{-3} m, r is the radius of rotation of the fiber-optic probe, equal to 6×10^{-3} m, and L is the coordinate direction along the line of sight of the detector, marking the length of the scattering volume as shown in Fig. 4. The pathlength of the radiation reaching the

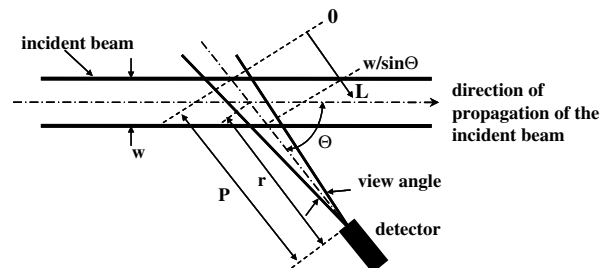


Fig. 4 – Coordinate system used in recovering the scattering phase function from the measured intensity distribution [26].

detector is denoted by $P = w/2\sin\theta + r$ [22]. Note that due to the finite size of the probe and the beam, data could only be obtained for scattering angle θ up to 160° where the probe did not obstruct the incident beam.

The extinction coefficient $\beta_{632.8}$ was measured with the nephelometer at wavelength 632.8 nm. In this method, the radiation flux $F_\lambda(z)$, expressed in W m^{-2} , at two different locations z_1 and z_2 along the path of a divergent incident beam are measured. The extinction coefficient was evaluated as [22],

$$\beta_{632.8} = \frac{\ln|F_{632.8}(z_2)/F_{632.8}(z_1)| + \ln|z_1^2/z_2^2|}{z_1 - z_2} \quad (13)$$

where z is the distance between the detector and the virtual image of the last lens in the optical setup shown in Fig. 4. Note that the second term in the numerator accounts for the divergence of the incident beam. At all angles, the experimental value of $\beta_{632.8}P$ was less than 0.1 ensuring single scattering [22].

Then, the extinction coefficients β_λ of the four strains of *C. reinhardtii* were measured from normal-normal transmittance measurements $T_{\lambda,x}$ over the spectral range from 300 to 1300 nm using a UV-VIS-NIR spectrophotometer (Model UV-3101PC, Shimadzu, USA). All the transmission measurements were carried out in a liquid flow cell of pathlength t equal to 0.001 m with quartz windows (FT04-060 by Thermo, USA).

During the measurements, the microorganism suspension was continuously flown through the flow cell with a peristaltic pump (4049 K33 by McMaster, USA) at a flow rate of approximately 10 mL min^{-1} to avoid settling of microorganisms. In order to account for reflection and refraction by the flow cell, measurements were made with respect to the transmission spectrum of PBS alone denoted by $T_{\lambda,\text{PBS}}$.

Due to its large acceptance angle of about 3° , the spectrophotometer measured an apparent extinction coefficient χ_λ given as [17,32]

$$\chi_\lambda = -\frac{1}{t} \ln\left(\frac{T_{\lambda,X}}{T_{\lambda,\text{PBS}}}\right) \quad (14)$$

The apparent extinction coefficient is related to the true absorption and extinction coefficients through [17,32],

$$\chi_\lambda = \kappa_\lambda + \sigma_\lambda - \varepsilon_n \sigma_\lambda \quad (15)$$

where ε_n represents the portion of the light scattered in the forward direction and detected by the spectrophotometer in directions other than the normal direction due to the finite size of the acceptance angle. It is defined as [42,43],

$$\varepsilon_n = \frac{1}{2} \int_0^{\theta_a} \Phi_\lambda(\theta) \sin\theta \, d\theta \quad (16)$$

where θ_a is the half acceptance angle of the detector. Using Eq. (15), the extinction coefficient can be determined as

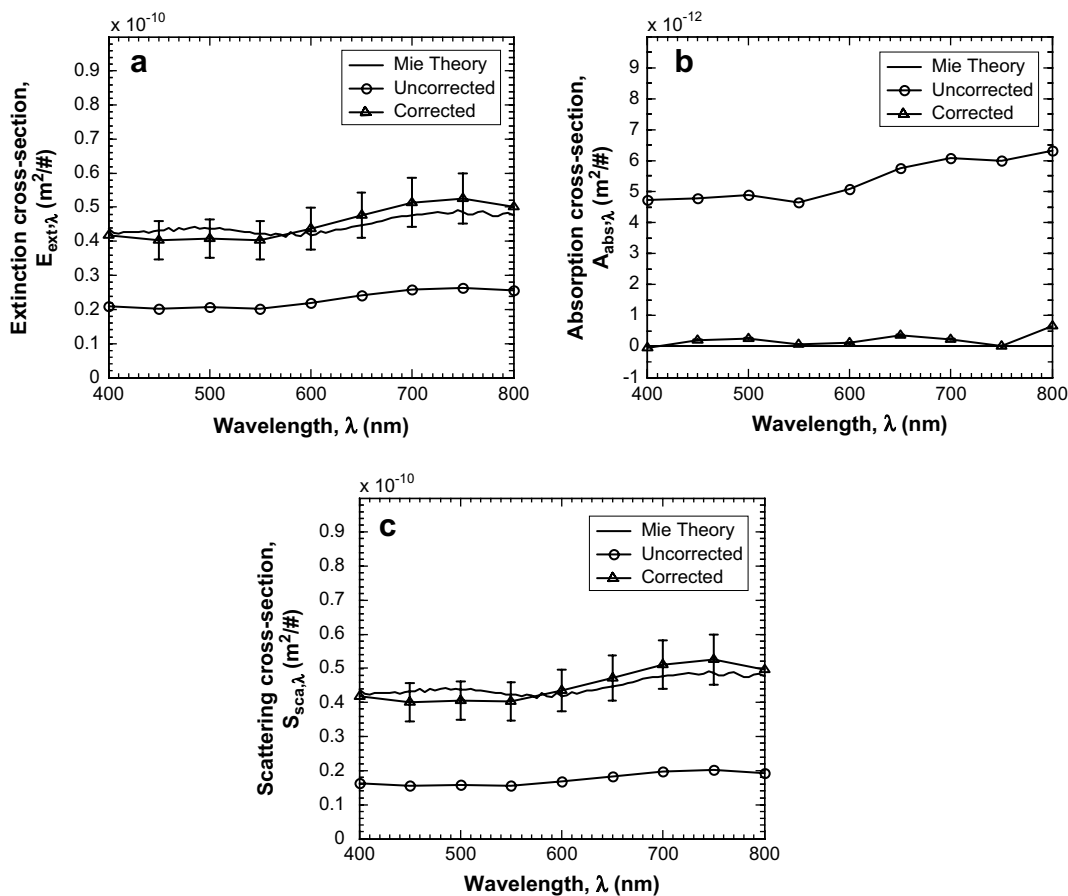


Fig. 5 – Comparison of the experimentally measured uncorrected and corrected (a) extinction, (b) absorption, and (c) scattering cross-sections of $5 \mu\text{m}$ diameter polystyrene microspheres with those predicted by the Mie theory.

$$\beta_\lambda = \frac{\chi_\lambda - \varepsilon_n \kappa_\lambda}{1 - \varepsilon_n} \quad (17)$$

Finally, the absorption coefficient κ_λ was determined from the hemispherical transmittance measurements performed with an integrating sphere [22]. The measurements were corrected for scattering errors using the analysis suggested by Davies-Colley et al. [17]. Under single scattering conditions, the apparent absorption coefficient $\chi_{h,\lambda}$ is related to the hemispherical transmittance of the microorganism sample $T_{h,\lambda,X}$ by [17]

$$\chi_{h,\lambda} = -\frac{1}{t} \ln \left(\frac{T_{h,\lambda,X}}{T_{h,\lambda,PBS}} \right) \quad (18)$$

where $T_{h,\lambda,PBS}$ is the normal-hemispherical transmittance of the PBS solution alone. Due to the geometry of the experimental set-up all the scattered radiation cannot be captured and measured by the integrating sphere. Thus, $\chi_{h,\lambda}$ overestimates the actual absorption coefficient that can be retrieved as [17],

$$\kappa_\lambda = \chi_{h,\lambda} - (1 - \varepsilon_h) \sigma_\lambda \quad (19)$$

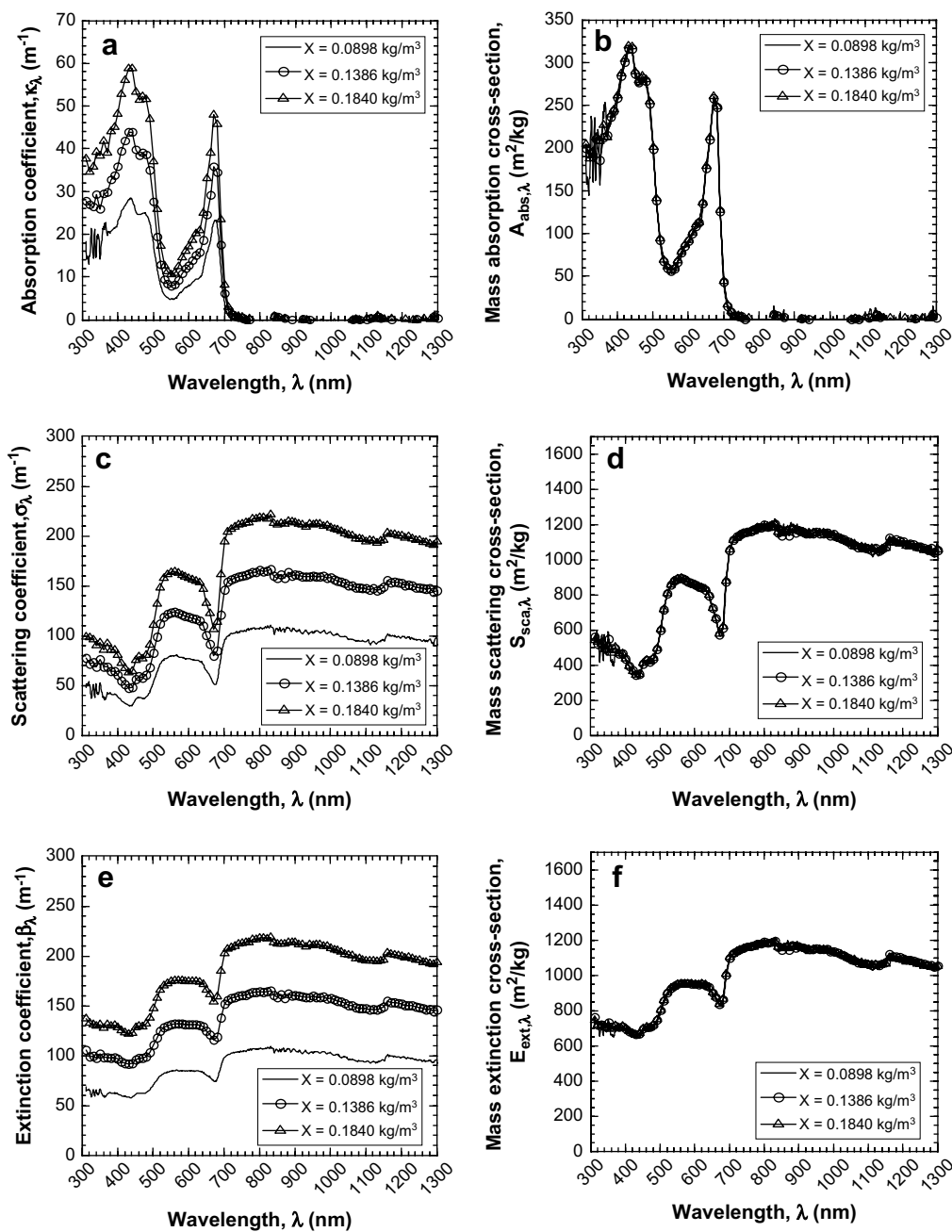


Fig. 6 – The (a) absorption κ_λ , (c) scattering σ_λ , and (d) extinction β_λ coefficients and the corresponding (b) mass absorption $A_{\text{abs},\lambda}$, (d) mass scattering $S_{\text{sca},\lambda}$, and (f) mass extinction $E_{\text{ext},\lambda}$ cross-sections of *C. reinhardtii* CC125 over the spectral range from 300 to 1300 nm at three different microorganism concentrations.

where ε_h is the fraction of scattered light detected by the integrating sphere. Ideally, ε_h is equal to unity when all light scattered in all directions is collected and detected by the integrating sphere. In order to account for the scattering error, Davies-Colley et al. [17] assumed that the microorganisms do not absorb radiation at wavelength λ_o , in this case $\lambda_o = 750$ nm for *Anabaena variabilis* and $\lambda_o = 900$ nm for *Rhodobacter sphaeroides*. At this wavelength, the apparent absorption coefficient is equal to the scattering error given as

$$\chi_{h,\lambda_o} = (1 - \varepsilon_h)\sigma_{\lambda_o} \quad (20)$$

Combining Eqs. (19) and (20) yields

$$\kappa_\lambda = \chi_{h,\lambda} - \chi_{h,\lambda_o} \frac{\sigma_\lambda}{\sigma_{\lambda_o}} \quad \text{where} \quad \frac{\sigma_\lambda}{\sigma_{750}} = \frac{\chi_\lambda - \chi_{h,\lambda}}{\chi_{750} - \chi_{h,750}} \quad (21)$$

3.3. Validations

First, measurements using the nephelometer and the procedure to analyze the data have been successfully validated with polystyrene spheres of 19 μm in diameter and with glass fibers of 10 mm in length and 17 μm in diameter as reported in Ref. [41].

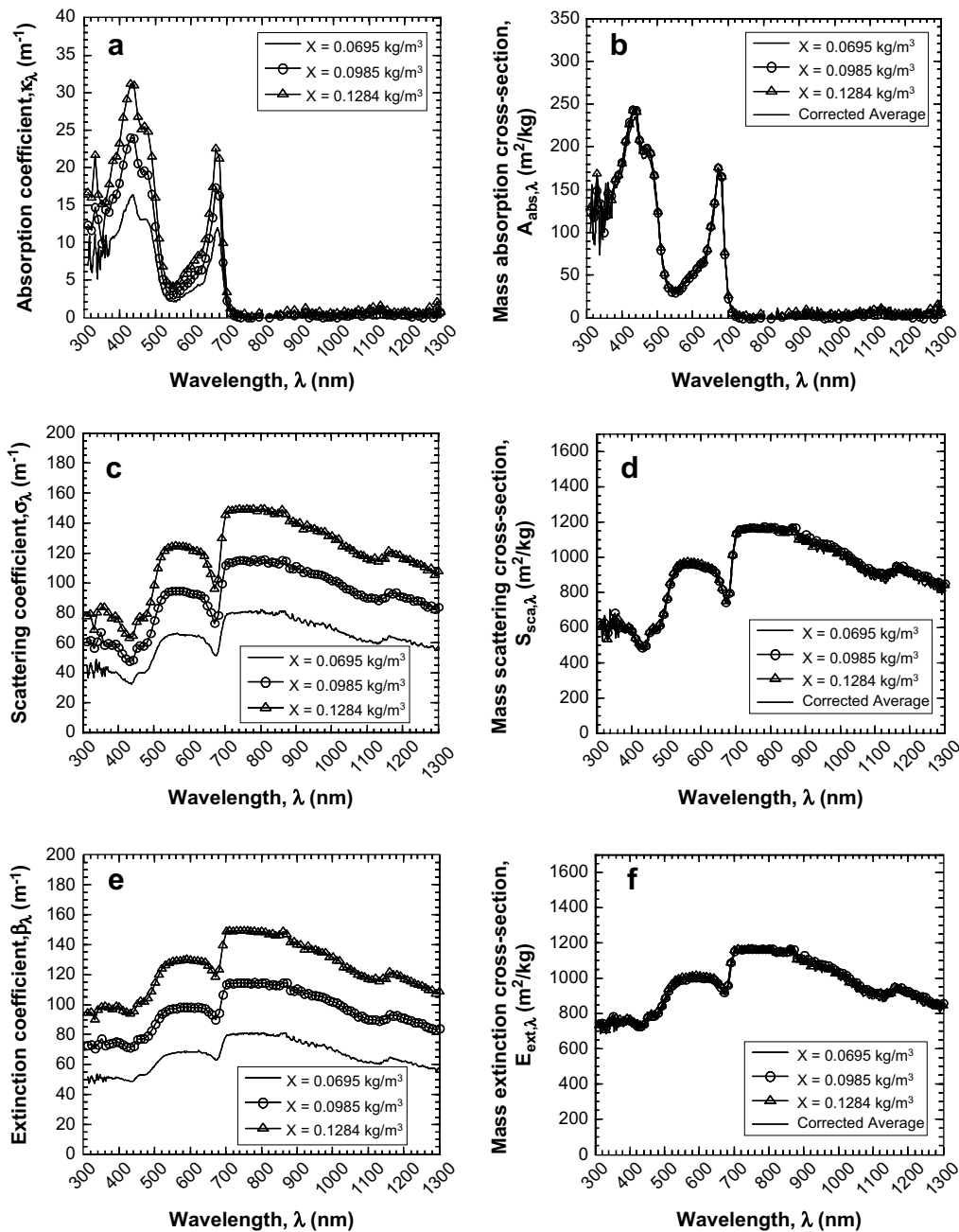


Fig. 7 – The (a) absorption κ_λ , (c) scattering σ_λ , and (d) extinction β_λ coefficients and the corresponding (b) mass absorption $A_{\text{abs},\lambda}$, (d) mass scattering $S_{\text{sca},\lambda}$ and (f) mass extinction $E_{\text{ext},\lambda}$ cross-sections of *C. reinhardtii tla1* over the spectral range from 300 to 1300 nm at three different microorganism concentrations.

The experimental set-up and analysis for measuring the extinction, absorption and scattering coefficients have also been successfully validated against predictions from Mie theory using polystyrene microspheres with diameter of 5 μm and standard deviation of 0.6 μm supplied by Duke Scientific Corp., USA (Part No: 2005A). Fig. 5 compares the extinction, absorption and scattering cross-sections of the microspheres predicted by Mie theory with the uncorrected experimental results [using Eqs. (14) and (18)] and the corrected results [using Eqs. (17) and (21)] over the spectral range from 400 to 800 nm. It shows that predictions from Mie theory lie within the experimental uncertainty of the corrected experimental

data estimated to be 14% for both the extinction and scattering cross-sections and within 6% for the absorption cross-section. The experimental uncertainties in cross-sections were estimated from the propagation of uncertainties in measuring the normal-normal and normal-hemispherical transmittances, the factors ϵ_n and ϵ_h , and the concentration of the polystyrene microspheres. Note that in our Mie theory calculations, the spheres were assumed to be non-absorbing, i.e., their absorption cross-section was equal to zero over the entire spectral range of interest (Fig. 5b).

In summary, the experimental apparatus and data analysis procedure were successfully validated. It has been established

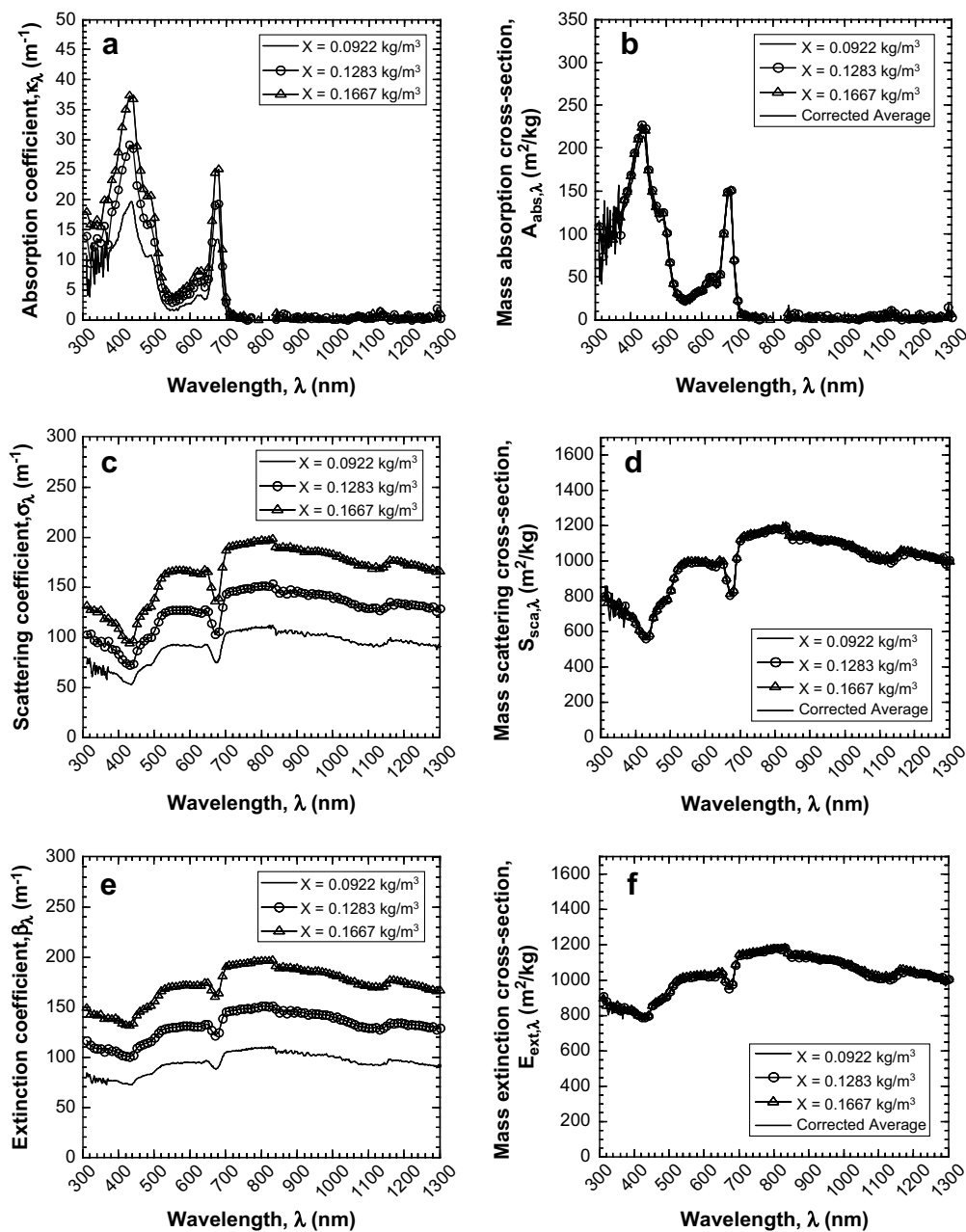


Fig. 8 – The (a) absorption κ_λ , (c) scattering σ_λ , and (d) extinction β_λ coefficients and the corresponding (b) mass absorption $A_{\text{abs},\lambda}$, (d) mass scattering $S_{\text{sca},\lambda}$ and (f) mass extinction $E_{\text{ext},\lambda}$ cross-sections of *C. reinhardtii* tlaX over the spectral range from 300 to 1300 nm at three different microorganism concentrations.

that correcting for the forward scattering is necessary for accurately measuring both the extinction and the absorption coefficients. The experimental results reported from here on correspond to the corrected data.

4. Results and discussion

All transmittance measurements were performed twice and the arithmetic average of the results is reported. The relative difference between the replica measurements was less than 0.1% over the entire spectral region considered and for all microorganisms.

4.1. Cross-sections of the wild strain

Fig. 6(a), (c), and (e) shows the absorption κ_λ , scattering σ_λ , and extinction β_λ coefficients of *C. reinhardtii* CC125, respectively, measured at three different microorganism concentrations, namely 0.0898, 0.1386, and 0.1840 kg m^{-3} in the spectral region from 300 to 1300 nm. Fig. 6(a) shows that *C. reinhardtii* CC125 have absorption peaks at 435, 475, and 676 nm. The peaks at 435 nm and 676 nm correspond to the absorption peaks of in vivo chlorophyll *a*. In addition, in vivo chlorophyll *b* has absorption peaks at 475 and 650 nm. Thus, the absorption peak at 475 nm and the peak broadening around 650 nm observed in Fig. 6(a) can be attributed to the presence of

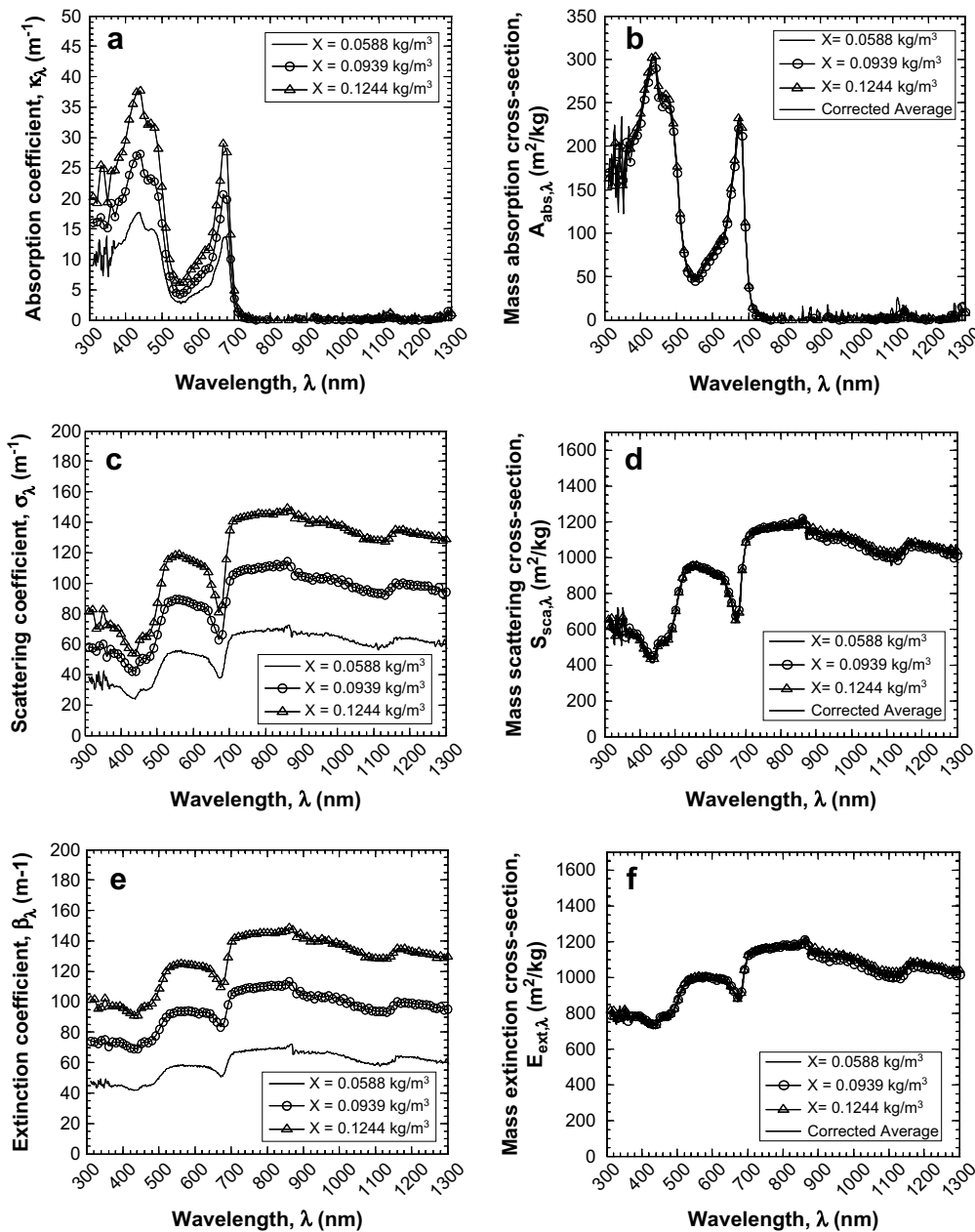


Fig. 9 – The (a) absorption κ_λ , (c) scattering σ_λ , and (d) extinction β_λ coefficients and the corresponding (b) mass absorption $A_{\text{abs},\lambda}$, (d) mass scattering $S_{\text{sca},\lambda}$ and (f) mass extinction $E_{\text{ext},\lambda}$ cross-sections of *C. reinhardtii* tla1-CW⁺ over the spectral range from 300 to 1300 nm at three different microorganism concentrations.

chlorophyll b. The chlorophyll a and b pigments are responsible for absorbing solar radiation and generating electrons that drive the metabolic reactions of the microorganisms.

In addition, Fig. 6(b), (d), and (f) shows the spectral mass absorption, mass scattering and mass extinction cross-sections $A_{\text{abs},\lambda}$, $S_{\text{sca},\lambda}$ and $E_{\text{ext},\lambda}$ over the spectral region from 300 to 1300 nm. It establishes that $A_{\text{abs},\lambda}$, $S_{\text{sca},\lambda}$ and $E_{\text{ext},\lambda}$ are independent of concentration X as they collapse on a single line for different microorganism concentrations. This also shows that multiple scattering is negligible for the concentrations considered as assumed in the data analysis.

4.2. Cross-sections of the transformants

The coefficients κ_λ , σ_λ and β_λ and the cross-sections $A_{\text{abs},\lambda}$, $S_{\text{sca},\lambda}$ and $E_{\text{ext},\lambda}$ of the strains *tla1*, *tlaX* and *tla1-CW⁺* were obtained in a similar manner and are presented in Figs. 7 to 9, respectively. The general trends observed and the absorption peaks for the genetically engineered strains are similar to those found for the wild strain.

4.3. Comparisons between the wild strain and the transformants

In order to better appreciate the effect of genetic engineering on the radiation characteristics of the truncated chlorophyll antenna transformants, Fig. 10(a) through (c) shows the ratio

of cross-sections $A_{\text{abs},\lambda}$, $S_{\text{sca},\lambda}$ and $E_{\text{ext},\lambda}$ of *tla1*, *tla1-CW⁺* and *tlaX* to those of CC125, respectively. Fig. 10(a) indicates that genetic engineering of *C. reinhardtii* CC125 reduces the absorption cross-section $A_{\text{abs},\lambda}$ (i) by 25% to 45% for *tla1*, (ii) by 30% to 70% for *tlaX*, and (iii) by 5% to 15% for *tla1-CW⁺* over the spectral region from 400 to 700 nm, i.e., PAR. Note that the ratio of cross-sections with respect to those of the wild strain outside PAR gives very large and noisy results due to division by zero or very small numbers. Furthermore, these trends agree well with the measured chlorophyll concentrations of the strains summarized in Table 2. Moreover, for all wavelengths between 400 and 700 nm, *tlaX* absorbs less than *tla1* as expected a priori. This is especially apparent around the absorption peaks of chlorophyll b at 475 and 650 nm.

On the other hand, changes in the mass scattering cross-sections show an opposite trend to those observed for the mass absorption cross-sections. Fig. 10(b) shows that the scattering cross-sections of *tla1*, *tlaX* and *tla1-CW⁺* increase by up to 45%, 80% and 25%, respectively. The maximum increase is observed around the absorption peaks of *C. reinhardtii* CC125 at 435, 475 and 676 nm. Thus, as absorption is reduced, scattering becomes more important for the genetically engineered *C. reinhardtii*. Similar observations have been reported in the ocean optics literature where decrease in the absorption cross-section is associated with an increase in the scattering cross-section [32]. Moreover, while CC125, *tlaX* and *tla1-CW⁺* display similar scattering cross-sections in the spectral region

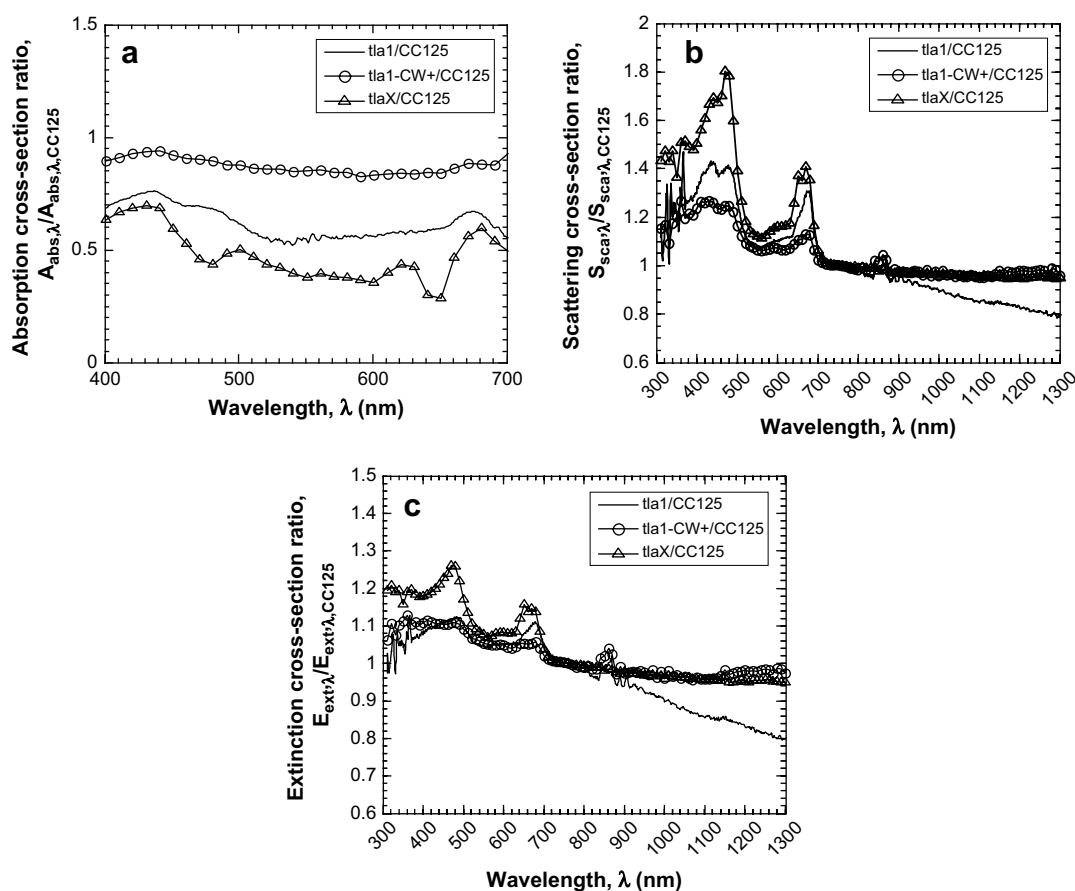


Fig. 10 – The ratio of the (a) mass absorption $A_{\text{abs},\lambda}$ (b) mass scattering $S_{\text{sca},\lambda}$ (c) mass extinction cross-sections $E_{\text{ext},\lambda}$ of *tla1*, *tla1-CW⁺* and *tlaX* with respect to those of *C. reinhardtii* CC125.

from 700 to 1,300 nm, *tla1* feature a smaller scattering cross-section that decreases with increasing wavelength. This can be attributed to the fact that *tla1* lack cell walls the other strains have.

Moreover, Fig. 10(c) illustrates the ratio of the extinction cross-section $E_{\text{ext},\lambda}$ of *tla1*, *tlaX* and *tla1-CW⁺* with respect to that of CC125. It shows that $E_{\text{ext},\lambda}$ for *tla1* and *tla1-CW⁺* do not differ by more than 10% from that of CC125 in the spectral region from 300 to 700 nm. On the other hand, the extinction cross-section of *tlaX* increases as much as 25%. Furthermore, the extinction cross-sections of the strains with cell walls are identical in the spectral region from 700 to 1300 nm. However, similar to the scattering cross-sections, the extinction cross-section of *tla1* decreases with increasing wavelength with respect to those of the strains with cell walls. Although chlorophyll antenna reduction does not reduce the extinction cross-sections of the mutants, it has several advantages enabling improved photosynthetic efficiency. First of all, reduction in chlorophyll antenna size increases the saturation irradiance of photosynthesis [9]. Thus, microorganisms can conduct photosynthesis at larger irradiances without incurring photooxidative damage. Note that the results of Polle et al. [19] were conducted at very large irradiance of $1500 \mu\text{mol m}^{-2} \text{s}^{-1}$. Moreover, reducing the chlorophyll antenna size increases the quantum efficiency of photosynthesis at large irradiances [8]. This is because, photons are not absorbed and wasted as heat and fluorescence by a given microorganism but scattered, mainly in the forward direction, increasing their chance of being used by other microorganisms. Finally, since scattering is mainly in the forward direction, the effect of larger scattering cross-section on the local irradiance within the photobioreactor is not trivial and requires detailed radiation transfer analysis. However, this analysis falls beyond the scope of the present study.

The single scattering albedo ω_λ represents the contribution of scattering to the overall extinction and is shown in Fig. 11(a) for all strains. The figure establishes that the single scattering albedo for all strains is greater than 0.5 and scattering dominates over absorption over the entire spectrum. Then, accurate knowledge of the scattering phase function $\phi_\lambda(\theta)$ of the microorganisms and solution of the RTE are required for accurate simulation, modeling and optimization of the photobioreactor as established by Berberoğlu et al. [14]. In particular, the commonly used Beer-Lambert's law is no longer valid as it does not distinguish between absorption and scattering phenomena and ignores in-scattering (path radiance) represented by the second term on the right-hand side of Eq. (1) [14]. Furthermore, to better illustrate the effect of genetic engineering on ω_λ Fig. 11(b) shows the ratio of the single scattering albedo of all strains with respect to that of the wild strain CC125. It indicates that ω_λ is larger than that of CC125 by up to 30%, 45% and 15% for *tla1*, *tlaX* and *tla1-CW⁺*, respectively.

4.4. Scattering phase functions of all strains

Finally, the scattering phase functions of all strains were measured using the nephelometer at microorganism concentrations of $0.007 \pm 0.002 \text{ kg m}^{-3}$ and at the wavelength of 632.8 nm. Fig. 12 shows the scattering phase functions of

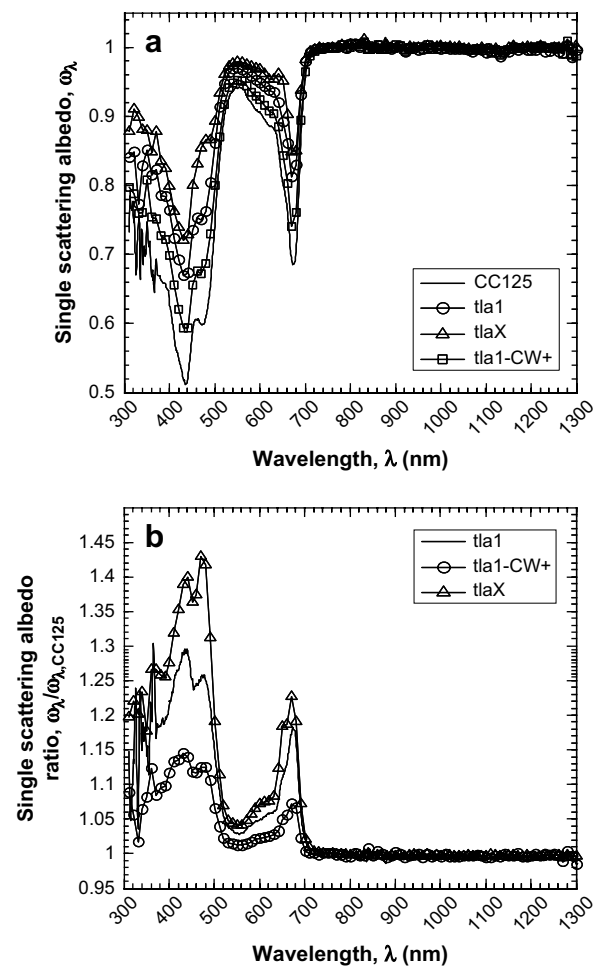


Fig. 11 – (a) The single scattering albedo ω_λ for all strains and (b) the ratio of the single scattering albedo of *tla1*, *tlaX* and *tla1-CW⁺* with respect to that of *C. reinhardtii* CC125 over the spectral range from 300 to 1300 nm.

CC125, *tla1*, *tlaX* and *tla1-CW⁺* measured by the nephelometer along with the truncated phase function (TPF) approximations. In TPF, the phase function is divided into two parts, from 0 to θ_{cutoff} and from θ_{cutoff} to π . Each part is a linear combination of two Henyey–Greenstein phase functions. The latter is given as [15]

$$\Phi_{\text{HG}} = \frac{1 - g^2}{[1 + g^2 - 2g \cos \theta]^{3/2}} \quad (22)$$

where g is the mean cosine of the scattering phase function, also known as the Henyey–Greenstein asymmetry factor. The TPF for the different strains is expressed as [14]

$$\begin{aligned} \Phi(\theta) &= f_1 \Phi_{\text{HG},g_{\text{TPF},1}}(\theta) + (1 - f_1) \Phi_{\text{HG},g_{\text{TPF},2}} \quad \text{for } 0 \leq \theta \leq \theta_{\text{cutoff}} \\ \Phi(\theta) &= h_1 [f_1 \Phi_{\text{HG},g_{\text{TPF},1}}(\theta) + (1 - f_1) \Phi_{\text{HG},g_{\text{TPF},2}}] \quad \text{for } \theta_{\text{cutoff}} < \theta < \pi \end{aligned} \quad (23)$$

where f_1 and h_1 are weighing parameters and $g_{\text{TPF},1}$, and $g_{\text{TPF},2}$ are the asymmetry factors. These are determined by minimizing the sum of the squares of the error between

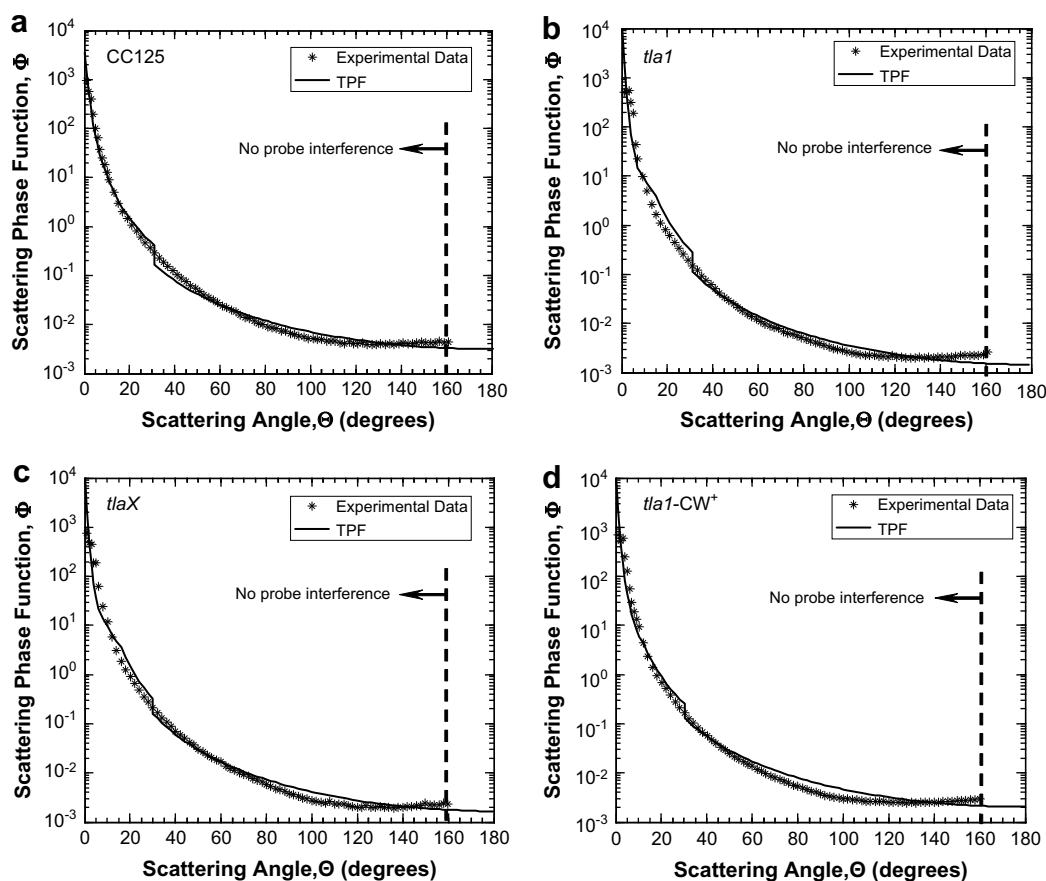


Fig. 12 – The scattering phase function of (a) CC125, (b) *tla1*, (c) *tlaX* and (d) *tla1-CW*⁺ at 632.8 nm obtained experimentally and the corresponding TPF approximation.

experimentally obtained phase function and the TPF model. Note that the TPF function needs to be normalized by the method previously adopted by Nicolau et al. [44]. The TPF parameters along with the Henyey–Greenstein asymmetry factors for all strains are summarized in Table 3. Fig. 12 indicates that the scattering is mainly in the forward direction for all strains. Moreover, the scattering phase functions of all strains show similar trends. Finally, the TPF parameters indicate that the scattering phase function of the genetically engineered strains is peaked slightly more forward than the wild strain.

Table 3 – Parameters associated with the TPF and Henyey–Greenstein approximations for the scattering phase function of all strains at 632.8 nm				
	CC125	<i>tla1</i>	<i>tlaX</i>	<i>tla1-CW</i> ⁺
$g_{TPF,1}$	0.98	0.99	0.99	0.99
$g_{TPF,2}$	0.95	0.96	0.98	0.97
f_1	0.65	0.86	0.72	0.71
h_1	0.42	0.40	0.50	0.52
θ_{cutoff} (°)	30	30	30	30
g	0.98	0.99	0.99	0.98

5. Conclusions

This article presents for the first time the radiation characteristics of *C. reinhardtii* CC125 and its truncated chlorophyll antenna transformants *tla1*, *tlaX* and *tla1-CW*⁺ over the spectral range from 300 to 1,300 nm as well as their scattering phase functions at 632.8 nm. It establishes that *C. reinhardtii* CC125 has major absorption peaks at 435 and 676 nm, corresponding to the in vivo absorption peaks of chlorophyll *a*, and at 475 and 650 nm corresponding to that of chlorophyll *b*. The genetically engineered strains have less chlorophyll pigments than the wild strain and thus have smaller absorption cross-sections. In particular, *tlaX* has the smallest absorption cross-section and the lowest chlorophyll *b* concentration of all strains. However, the reduction in the absorption cross-section is compensated by an increase in scattering cross-section of the genetically engineered strains.

Moreover, the single scattering albedo ω_s is greater than 0.5 over the spectral region from 300 to 1300 nm, indicating that scattering is the dominant phenomena contributing to the overall extinction. Although scattering dominates over absorption, it is mainly in the forward direction and reduction of absorption cross-section can still improve the performance of photobioreactors by increasing the saturation irradiance of algae and quantum efficiency of photobiological hydrogen

production. Thus, optimizing light transport in the photobioreactor requires careful radiation transfer analysis [14]. The reported radiation characteristics should enable such accurate radiation transfer modeling of photobioreactors for hydrogen production. Finally, the experimental and analytical methods presented here can be used to accurately measure the radiation characteristics of other microorganisms for photobioreactors or ocean optics applications. Future work should evaluate the specific hydrogen production rate and light to hydrogen energy conversion efficiency of the genetically engineered microorganisms to ensure that pigment reduction has not adversely affected their hydrogen production metabolism.

Acknowledgements

The authors gratefully acknowledge the DOE HFC&IT Program for the generation of *tla1*, *tlaX* and *tla1-CW⁺* as well as the support of the California Energy Commission through the Energy Innovation Small Grant (EISG 53723A/03-29; Project Manager: Michelle McGraw).

REFERENCES

- [1] Pulz O. Photobioreactors: production systems for phototrophic microorganisms. *Appl Microbiol Biotechnol* 2001;57(3):287–93.
- [2] Kim NJ, Suh IS, Hur BK, Lee CG. Simple monodimensional model for linear growth rate of photosynthetic microorganisms in flat-plate photobioreactors. *J Microbiol Biotechnol* 2002;12:962–71.
- [3] Markov SA, Lichtl R, Rao KK, Hall DO. A hollow fibre photobioreactor for continuous production of hydrogen by immobilized cyanobacteria under partial vacuum. *Int J Hydrogen Energy* 1993;18:901–6.
- [4] Markov SA, Bazin MJ, Hall DO. Hydrogen photoproduction and carbon dioxide uptake by immobilized *Anabaena variabilis* in a hollow-fiber photobioreactor. *Enzyme Microbiol Technol* 1995;17:306–10.
- [5] Markov SA, Thomas AD, Bazin MJ, Hall DO. Photoproduction of hydrogen by cyanobacteria under partial vacuum in batch culture or in a photobioreactor. *Int J Hydrogen Energy* 1997; 22:521–4.
- [6] Tsygankov AA, Fedorov AS, Kosourov SN, Rao KK. Hydrogen production by cyanobacteria in an automated outdoor photobioreactor under aerobic conditions. *Biotechnol Bioeng* 2002;80:777–83.
- [7] Yoon JH, Shin JH, Kim MS, Sim SJ, Park TH. Evaluation of conversion efficiency of light to hydrogen energy by *Anabaena variabilis*. *Int J Hydrogen Energy* 2006;31:721–7.
- [8] Melis A. Green alga hydrogen production: process, challenges and prospects. *Int J Hydrogen Energy* 2002;27:1217–28.
- [9] Melis A, Neidhardt J, Benemann JR. *Dunaliella salina* (Chlorophyta) with small chlorophyll antenna sizes exhibit higher photosynthetic productivities and photon use efficiencies than normally pigmented cells. *J Appl Phycol* 1999;10:515–25.
- [10] Cornet JF, Dussap CG, Dubertret G. A structured model for simulation of cultures of the cyanobacterium *Spirulina platensis* in photobioreactors. I. Coupling between light transfer and growth kinetics. *Biotechnol Bioeng* 1992;40:817–25.
- [11] Cornet JF, Dussap CG, Cluzel P, Dubertret G. A structured model for simulation of cultures of the cyanobacterium *Spirulina platensis* in photobioreactors. II. Identification of kinetic parameters under light and mineral limitations. *Biotechnol Bioeng* 1992;40:826–34.
- [12] Cornet JF, Dussap CG, Gross JB, Binois C, Lasseur C. A simplified monodimensional approach for modeling coupling between radiant light transfer and growth kinetics in photobioreactors. *Chem Eng Sci* 1995;50:1489–500.
- [13] Melis A, Zhang L, Forestier M, Ghirardi ML, Seibert M. Sustained photobiological hydrogen gas production upon reversible inactivation of oxygen evolution in the green alga *Chlamydomonas reinhardtii*. *Plant Physiol* 2000;117:129–39.
- [14] Berberoğlu H, Yin J, Pilon L. Simulating light transfer in a bubble sparged photobioreactor for simultaneous hydrogen fuel production and CO₂ mitigation. *Int J Hydrogen Energy* 2007;32:2273–85.
- [15] Modest MF. Radiative heat transfer. San Diego (CA): Academic Press; 2003.
- [16] Stramski D, Mobley CD. Effect of microbial particles on oceanic optics: a database of single-particle optical properties. *Limnol Oceanogr* 1997;42:538–49.
- [17] Davies-Colley RJ, Pridmore RD, Hewitt JE. Optical properties and reflectance spectra of 3 shallow lakes obtained from a spectrophotometric study. *N Z J Mar Freshwater Res* 1983; 17:445–59.
- [18] BricaudMorel A, Prieur L. Optical efficiency factors of some phytoplankters. *Limnol Oceanogr* 1983;28:816–32.
- [19] Polle JE, Kanakagiri SD, Melis A. *tla1*, a DNA insertional transformant of the green alga *Chlamydomonas reinhardtii* with a truncated light-harvesting chlorophyll antenna size. *Planta* 2003;217:49–59.
- [20] Polle JE, Benemann JR, Tanaka A, Melis A. Photosynthetic apparatus organization and function in the wild type and a chlorophyll *b*-less mutant of *Chlamydomonas reinhardtii*: dependence on carbon source. *Planta* 2000;211:335–44.
- [21] Ke B. Photosynthesis, photobiochemistry and photobiophysics. Dordrecht, The Netherlands: Kluwer Academic Publishers; 2001.
- [22] Privoznik KG, Daniel KJ, Incropera FP. Absorption, extinction, and phase function measurements for algal suspensions of *Chlorella pyrenoidosa*. *J Quantit Spectrosc Radiat Transfer* 1978;20:345–52.
- [23] Bohren CF. Multiple scattering of light and some of its observable consequences. *Am J Phys* 1986;55:524–33.
- [24] Jonasz M, Fournier GR. Light scattering by particles in water: theoretical and experimental foundations. San Diego (CA): Academic Press; 2007.
- [25] Bohren CF, Huffman DR. Absorption and scattering of light by small particles. New York (NY): John Wiley & Sons; 1998.
- [26] Daniel KJ, Incropera FP. Optical property measurements in suspensions of unicellular algae. Purdue University Technical Report; 1977. HTL 77–4.
- [27] Moore C, Zeneveld RV, Kitchen JC. Preliminary results from an *in situ* spectral absorption meter. In: Ocean optics 11. Proceedings of SPIE, vol. 1750; 1992. p. 330–7.
- [28] Zaneveld JRV, Bartz R, Kitchen JC. Reflective tube absorption meter. In: Ocean optics 11. Proceedings of SPIE, vol. 1302; 1990. p. 124–36.
- [29] Maffione RA, Voss KJ, Honey RC. Measurement of the spectral absorption coefficient in the ocean with an isotropic source. *Appl Optics* 1993;32:3273–9.
- [30] Fry ES, Kattawar GW, Pope RM. Integrating cavity absorption meter. *Appl Optics* 1992;31:2055–65.
- [31] Bennet GT, Fry ES, Sogandares FM. Photothermal measurements of the absorption coefficient of water at 590 nm. In: Ocean optics 8. Proceedings of SPIE, 637; 1986. p. 172–80.

- [32] Davies-Colley RJ, Pridmore RD, Hewitt JE. Optical properties of some freshwater phytoplanktonic algae. *Hydrobiologia* 1986;133:165–78.
- [33] Stramski D, Piskozub J. Estimation of scattering error in spectrophotometric measurements of light absorption by aquatic particles from three-dimensional radiative transfer simulations. *Appl Optics* 2003;42:3634–46.
- [34] Merzlyak MN, Naqvi KR. On recording the true absorption spectrum and scattering spectrum of a turbid sample: application to cell suspensions of cyanobacterium *Anabaena variabilis*. *J Photochem Photobiol B* 2000;58:123–9.
- [35] Wintermans JF, De Mots A. Spectrophotometric characteristics of chlorophylls a and b and their pheophytins in ethanol. *Biochem. Biophys. Acta* 1965;109:448–53.
- [36] Harris EH. *The chlamydomonas sourcebook*. New York (NY): Academic Press; 1989.
- [37] Robinson JP. *Current protocols in cytometry*. New York (NY): John Wiley & Sons; 2001.
- [38] Chen HC, Melis A. Localization and function of SulP, a nuclear-encoded chloroplast sulfate permease in *Chlamydomonas reinhardtii*. *Planta* 2004;220:198–210.
- [39] Rasband WS. ImageJ. Bethesda (MD), USA: U.S. National Institute of Health, <http://rsb.info.nih.gov/ij/>; 1997–2007.
- [40] Yoon JH, Sim SJ, Kim MS, Park TH. High cell density culture of *Anabaena variabilis* using repeated injections of carbon dioxide for the production of hydrogen. *Int J Hydrogen Energy* 2002;27:1265–70.
- [41] Berberoğlu H, Pilon L. Experimental measurement of the radiation characteristics of *Anabaena variabilis* ATCC 29413-U and *Rhodobacter sphaeroides* ATCC 49419. *Int J Hydrogen Energy* 2007;32:4772–85.
- [42] Kokhanovsky AA. Scattered light corrections to sun photometry: analytical results for single and multiple scattering regimes. *J Opt Soc Am A* 2007;24:1131–7.
- [43] Agrawal BM, Mengüç MP. Forward and inverse analysis of single and multiple scattering of collimated radiation in an axisymmetric system. *Int J Heat Mass Transfer* 1991;34:633–47.
- [44] Nicolau VP, Raynaud M, Sacadura JF. Spectral radiative properties identification of fiber insulating materials. *Int J Heat Mass Transfer* 1994;37(Suppl. 1):311–24. <http://www.sciencedirect.com/science/article/B6V3H-481FXV6-KT/2/248fca2516c44385b2cb58d87eeaf81e>.